Boletín de la Sociedad Española de Cerámica y Vidrio
Vol 53, 6, 265-274, Noviembre-Diciembre 2014 ISSN 0366-3175. eISSN 2173-0431.
http://dx.doi.org/10.3989/cyv.322014

BOLETIN DE LA SOCIEDAD ESPAÑOLA DE
Cerámica y Vidrio
A R T I C U L O

Colloidal stability of $Ni(OH)_2$ in water and its dispersion into a ceramic matrix from the reaction media to obtain Ni/Al_2O_3 materials

S. CABANAS-POLO, B. FERRARI, A. J. SÁNCHEZ-HERENCIA

Instituto de Cerámica y Vidrio ICV – CSIC, c/ Kelsen, 5, 28049 Madrid, España.

Ni/Al_2O_3 composites have been fabricated by slip casting of concentrated Ni(OH)2/Al2O3 suspensions and subsequent *in situ* reduction to metallic nickel during sintering. For that, the synthesis assisted by ultrasound of both α- and β-$Ni(OH)_2$ polymorphs, as well as their colloidal stability, have been studied. The structural differences between both polymorphs have been thoroughly studied by means of XRD, FTIR, DTA-TG, SSA, SEM and TEM, in order to optimize the starting suspensions. This way, the IEP of both polymorphs have been established (9.7 y 12 for β- and α-$Ni(OH)_2$, respectively), as well as the optimal content of an anionic dispersant (PAA) to stabilize the particles (0.8 wt. % for beta phase and 3.0 wt. % for alpha phase). Three different Ni/Al_2O_3 composites, with a high dispersion degree of the metallic phase, have been obtained considering the potential vs. particles distance curve of the $Ni(OH)_2$, and their structure has been discussed in terms of the strength of the agglomerates and/or aggregates of the $Ni(OH)_2$.

Keywords: Colloidal stability, CerMet, Shaping, Suspensions, Synthesis

Estabilidad coloidal de $Ni(OH)_2$ en agua y su dispersión en una matriz cerámica desde el medio de reacción para la obtención de materiales Ni/Al_2O_3

La obtención de materiales compuestos Ni/Al_2O_3 se ha llevado a cabo mediante colaje en molde de escayola de suspensiones concentradas de $Ni(OH)_2/Al_2O_3$ y su posterior reducción *in situ* para obtener la fase metálica. Para ello, se ha estudiado la síntesis asistida por ultrasonido de los polimorfos α- y β-$Ni(OH)_2$, así como su comportamiento coloidal en medio acuoso. Las diferencias estructurales entre ambos polimorfos han sido estudiadas en detalle mediante XRD, FTIR, ATD-TG, SSA, MEB y MET, para poder optimizar las suspensiones de partida. De esta manera, se ha establecido el PIE de ambos polimorfos (9.7 y 12 para las fases β- y α-$Ni(OH)_2$, respectivamente), así como el contenido óptimo de un dispersante aniónico (PAA) para la estabilización de las partículas (0.8 % p/p para la fase beta y 3.0 % p/p para la fase alfa). Tres materiales compuestos Ni/Al_2O_3 diferentes, con un alto grado de dispersión de la fase metálica, han sido obtenidos en función de la curva de potenciales de interacción frente a distancia entre partículas del $Ni(OH)_2$ y su estructura se ha discutido en función de la fortaleza de los aglomerados y/o agregados del $Ni(OH)_2$.

Palabras clave: Estabilidad coloidal, CerMet, Conformado, Suspensiones, Síntesis

Cómo citar este artículo: Cabanas-Polo, S.; Ferrari, B. y Sánchez-Herencia, A. J. (2014): Colloidal stability of $Ni(OH)_2$ in water and its dispersion into a ceramic matrix from the reaction media to obtain Ni/Al_2O_3 materials, *Bol. Soc. Esp. Ceram. Vidr.*, 53 (6): 265-274. http://dx.doi.org/10.3989/cyv.322014

1. INTRODUCTION

The incorporation of a secondary metallic phase, both as nano- or microparticles, into a ceramic matrix, is the most common strategy used for the fabrication of metal-ceramic composite materials (CerMets) . A good dispersion of the minority phase and an intimate union between this phase and the matrix, are key to obtain advanced materials with special properties. Within the different metals that can be employed for the reinforcement of ceramic matrices, such as iron, nickel, molybdenum, tungsten, cobalt, etc. [1], nickel is the most commonly used due to its capacity to improve the catalytic and mechanical properties of the ceramic matrix [2]. This way, anodes for solid oxide fuel cells (SOFCs) can be obtained by achieving a high dispersion of nickel particles in porous ytria estabilized zirconia matrices [3,4], while for dense zirconia matrices, the incorporation of nickel particles leads to an enhanced of its mechanical properties [5]. The fabrication of graded structures for thermal barrier coatings (TBCs) is another example of advanced materials that can be achieved by the incorporation of nickel to ceramic matrices [6].

Different processing techniques can be used for the preparation of metal ceramic composites. Among them, colloidal processing offers the possibility to achieve a high dispersion degree of the secondary phase (in this case nickel) into the ceramic matrix (in this case alumina), what would

affect the final properties of the composite, for example by decreasing its threshold limit to obtain conductive materials. At the same time, complex microstructures such as multilayers or coatings (on the nanometer to micrometer range), can be prepared by colloidal processing techniques [7]. On the other hand, considering the different chemical nature of both phases, colloidal processing allows the employment of a non-metallic precursor for the nickel phase, e. g. nickel hydroxide, with a higher compatibility with the ceramic phase, which can be synthesized in situ and processed directly from the post-reaction media, favoring the incorporation of small particles through a bottom-up approach [8]. Subsequent sintering of the composite under reducing atmosphere leads to the reduction of nickel hydroxide to metallic nickel.

Nickel hydroxide ($Ni(OH)_2$) presents two polymorphs know as α- and β-$Ni(OH)_2$. While β-$Ni(OH)_2$ crystallizes in an hexagonal system isostructural with brucite ($Mg(OH)_2$), α-$Ni(OH)_2$ is a metastable phase that easily transforms to β-$Ni(OH)_2$ during the synthesis process or in a strong alkali media [9]. The most common synthesis method result in the obtaining of the beta phase [10] while the alpha phase requires high energy processes such as microwave [11] or ultrasond assisted synthesis [9,12].

Despite the importance of nickel hydroxide as positive electrode in alkaline rechargeable batteries [13,14], only few studies can be found on the colloidal stability in aqueous media [15,16]. Generally, colloidal stability of inorganic systems is achieved by the electrostatic repulsion between particles with the same charge, which prevents their agglomeration and sedimentation. In order for this interaction to take place, it is necessary that the particles posses enough superficial charge to be away from each other and avoid Van der Waal interaction which would create attraction and, therefore, would destabilize the suspension. If the repulsion forces between particles are not sufficiently high, their surface can be modified by changing the pH or adding surface modifiers (e. g. surfactants or dispersants) that modify the particles surface by an adsorption mechanism [16]. In this context, Meyer *et al*. [16] studied the dispersion of β-$Ni(OH)_2$ with platelet-like morphology in terms of the electrokinetic mobility using an aqueous medium and citrate ions as a stabilizer agent. In other works, Cabanas-Polo *et al*. [12] and Durand-Keklikian *et al*. [15], studied the influence of different additives in the preparation of nickel hydroxide by different synthesis methods. Regarding the colloidal stability of alumina, different studies have shown that stable suspensions of alumina and alumina/nickel can be prepared using an anionic polyacrylate [17,18].

Herein, the fabrication of Ni/Al_2O_3 composites by slip casting of concentrated alumina/nickel hydroxide suspensions, and further sintering in reducing atmosphere, is presented. Three different processing routes, depending on the "particles distance *vs*. potential" curves of the nickel hydroxide, have been considered. For that, the synthesis of $Ni(OH)_2$ is first described in detailed, followed by its colloidal stability in aqueous media and further mixture with the alumina powder.

2. EXPERIMENTAL PART

2.1. Synthesis and characterization of $Ni(OH)_2$

The synthesis of nickel hydroxide has been carried out through two different routes named route A and route B, respectively. In both cases, nickel hydroxide hexahydrated ($Ni(NO_3)_2{\cdot}6H_2O$; Panreac Química S.A.U., Spain) and ammonium hydroxide (Panreac Química S.A.U., Spain) were used as reactants, and a high intensity sonochemical probe (Ti horn, 24 kHz, 100 W/cm^2, UP 400s, Dr. Hielsecher, Alemania) was employed to carry out the experiments. For route A, a certain amount of $Ni(NO_3)_2{\cdot}6H_2O$, to obtained a final Ni^{2+} concentration of 0.65 M, was added to a 2 M ammonium hydroxide solution previously under sonication (sample ANH). In the case of route B, a homogeneous solution of $Ni(NH_3)_x^{2+}$ complexes was prepared by dissolving the proper amount of $Ni(NO_3)_2{\cdot}6H_2O$ to obtain a final Ni^{2+} concentration of 0.10 M in a 2 M ammonium hydroxide solution. The homogeneous $Ni(NH_3)_x^{2+}$ solution was then sonicated for 90 min (sample BNH). Powders obtained for both routes were filtered using polymeric filters (ø = 0.22 μm) and then washed several times with distilled water at pH 10 (adjusted using tetramethylammonium hydroxide, TMAH). Finally, the powders were dried at 60 ºC for 2 h.

The chemical composition of the samples was analyzed by X-ray diffraction using a Siemens D5000 diffractometer (Germany) with a Kristalloflex 710 generator (K_α (Cu) λ = 1.5405 Å; 40 KV; 30 mA; 2θ = 5-70) and Fourier transform infrared spectroscopy (FTIR), using KBr pellets and a Perkin Elmer Spectrum 100 with a Universal ATR and a spectrum spot light 200 microscope. Differential scanning calorimetric (DSC) and thermogravimetric analysis (TGA) were carried out with a SDT Q600 analyzer (TA instruments) at a heating rate of 5 ºC/minute from room temperature up to 600 ºC using an alumina crucible. Coupled to the DSC-TGA equipment there is a Thermo Scientific Nicolet 6700 FT-IR Spectrometer that allows the identification of gases generated during the DSC-TGA measurements. Specific surface area was measured with a Monosorb Surface Area MS-13 equipment (Quantachrome Corporation, USA)), density was calculated by helium pycnometry using a Monosorb Multipycnometer (Quantachrome Corporation (USA)), and BET diameter was calculated using the equation $D_{BET} = 6/(SSA{\cdot}\rho)$, where SSA is the specific surface area and ρ is the density of the powder. Finally, the morphology of the powders was examined by FE-SEM (Hitachi S-4700, Japan) and TEM (Hitachi H-7100, Japan).

2.2. Colloidal stabilty

Zeta potential measurements were carried out in a Zetasizer Nano ZS (Malvern Instruments Ltd., UK). Colloidal suspensions for zeta potential measurements were prepared in KCl 0.01 M, to maintain constant the ionic strength of the medium, and using a solid contents of 0.1 g/L. TMAH dilution was used to adjust the pH. Polyacrylic acid (M_w=2000, Acros Organics, USA, prepared in an ammonia solution with a molar ratio PAA/NH_3 of 1.5 in order to ensure the PAA dissociation) was used as anionic surfactant based on previous works on the colloidal stability of alumina [18] . Particle size measurements were also performed using a Zetasizer Nano zs (Malvern Instruments Ltd., UK).

2.3. Shaping and sintering of Ni/Al_2O_3 composites

For the fabrication of Ni/Al_2O_3 composites, a commercial alumina powder (Condea HPA05, USA), with a specific

surface area of 9.5 m^2/g, a particle size of D_{v50} = 0.35 μm and a density of 3.99 g/cm^3 was employed. The colloidal stability of the alumina was achieved by using the same dispersant (i.e. PAA), whose capability to disperse colloidal alumina has been previously established [18].

Suspensions with both $Ni(OH)_2$ and Al_2O_3 were prepared in aqueous media using a PAA content of 1.0 wt. % (with respect to the alumina powder [18]) and 3.0 wt. % (with respect to $Ni(OH)_2$). The total PAA content was established at 1.1 wt. % (with respect to all the powder in suspension). In all cases, 50 mL of suspension were used, with a solid content of 30 vol %. 6.7 wt. % of $Ni(OH)_2$, (equivalent to a 2.0 vol. % of final metallic nickel after sintering) and 98.0 vol % of Al_2O_3 were used to prepare the suspensions. Three different routes (named routes 1, 2 and 3), depending on the initial nickel precursor and its place in the particles distance *vs*. potential curve, were used. Porous alumina moulds were used to performed the slip casting in order to obtain the Ni/Al_2O_3 green bodies.

For each composite, the sintering process to consolidate the green bodies consisted in a heat treatment from room temperature to 1450 ºC, at a heating rate of 5 ºC/min, with a plateau of 2 h at the maximum temperature. The sintering atmosphere was a mixture of N_2/H_2 with a 2 vol. % of hydrogen to reduce $Ni(OH)_2$ to Ni^0. Density of green and sintered bodies was measured by Arquimedes method in water and mercury, respectively. The final microstructure of the sintered samples was observed by by FE-SEM (Hitachi S-4700, Japan).

3. RESULTS AND DISCUSSION

3.1. $Ni(OH)_2$ synthesis

Based on the pH vs. log [Ni^{2+}] diagram for a fixed ammonia concentration ([NH_3] = 2 M), the experimental pH of the solution reaches a value of approximately 11.5 when using [Ni^{2+}] = 0.1 M, where there is an equilibrium between $Ni(OH)_2$ and $Ni(NH_3)_6^{2+}$ [12]. If at this point ammonia concentration decreases, the pH decreases too leading the reaction to the precipitation of nickel hydroxide. In this experiment the decrease in ammonia concentration is induced by the effects of ultrasound in the reaction media and is based on a degassing process where the bubbles generated during cavitation, and that present high specific surface area, grow at expense of dissolved gasses within the liquid, in this case ammonia, up to a maximum volume. At this point, bubbles explode releasing the gas and, therefore, the pH decreases and nickel hydroxide precipitates [12,16].

Following route A, a green powder precipitates immediately when the nickel nitrate ([Ni^{2+}] = 0.65 M), is added to the ammonia solution under sonication (sample ANH). After filtering, washing and drying the powder a yield of 45 % is obtained and the liquid phase presents a light blue color what indicates that there is still Ni^{2+} remaining in solution. On the other hand, when ultrasound is applied to the homogeneous $Ni(NH_3)_x^{2+}$ complexes (route B), a green solid appears in solution after 10-15 minutes. Product was then collected after 90 min with a yield of 27 % (sample BNH).

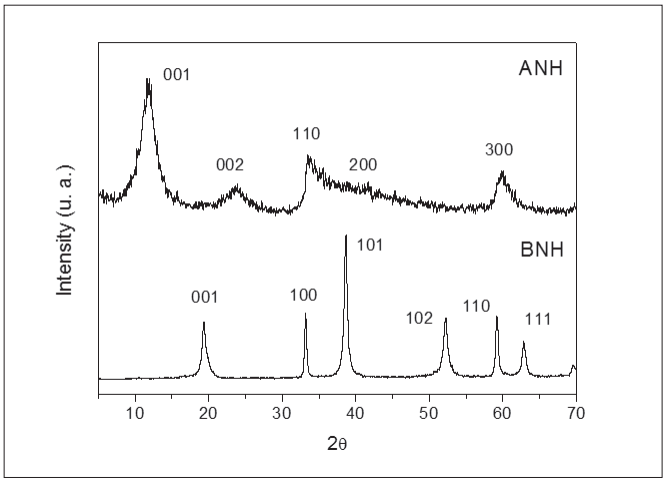

Figure 1. XRD of samples ANH and BNH.

Fig. 1 shows the X-ray diffraction patterns of the as-prepared samples, where it can be observed that sample ANH corresponds to the α-$Ni(OH)_2$ polymorph (indexed using JCPDS card 22-0444), while sample BNH was identified as β-$Ni(OH)_2$ (indexes using JCPDS card 14-0117). In both cases, pure products were obtained since there are no peaks of any impurity or mixtures of products. Sample BNH presents a well-defined diffractogram with sharp and narrow peaks typical of a well-crystallized phase, but in the case of sample ANH an abrupt diffractogram, characteristic of a turbostratic phase, with wider peaks is obtained (which is related to smaller crystallite sizes) [9,16,19].

Using the Warren modification of Scherrer formula [16], the crystallite size along the c-axis (L_{hkl}) was calculated from the XRD patterns of fig. 1. Results are shown in table 1 along with other morphological characteristics of the powders such as density (ρ), specific surface area (SSA) and BET diameter.

Considering the X-ray diffractograms of samples ANH and BNH, a smaller crystal size was expected for the alpha phase based on the wider peaks on the beta phase diffractogram, which was actually confirmed by the L_{hkl} values of table 1. This smaller crystal size observed for the alpha phase results in a smaller particle size for this sample, which is also corroborated by the BET diameter and the FESEM images of figure 2. In the images it can be seen how the alpha phase (fig. 2a) presents smaller particle agglomerates than the beta phase (fig. 2c). In addition, the morphology of the samples differs from one another. While sample ANH presents an open morphology that resembles to a sponge with diameters of around 0.4 μm, sample BNH is composed of flower-like aggregates ranging from 0.7 to 1.0 μm in diameter. In both cases, the thickness of the structures that conformed the agglomerates (sample ANH) or aggregates (sample BNH), are similar to the BET diameters

TABLE 1. CRYSTAL SIZE ALONG THE C AXIS, DENSITY, SPECIFIC SURFACE AREA AND BET DIAMETER OF SAMPLES ANH AND BNH.

Sample	XRD	L_{hkl} (nm)	ρ (g/cm^3)	SSA (m^2/g)	D_{BET} (nm)
ANH	α	3.5	2.7	73.0	30.0
BNH	β	13.3	3.9	30.3	51.0

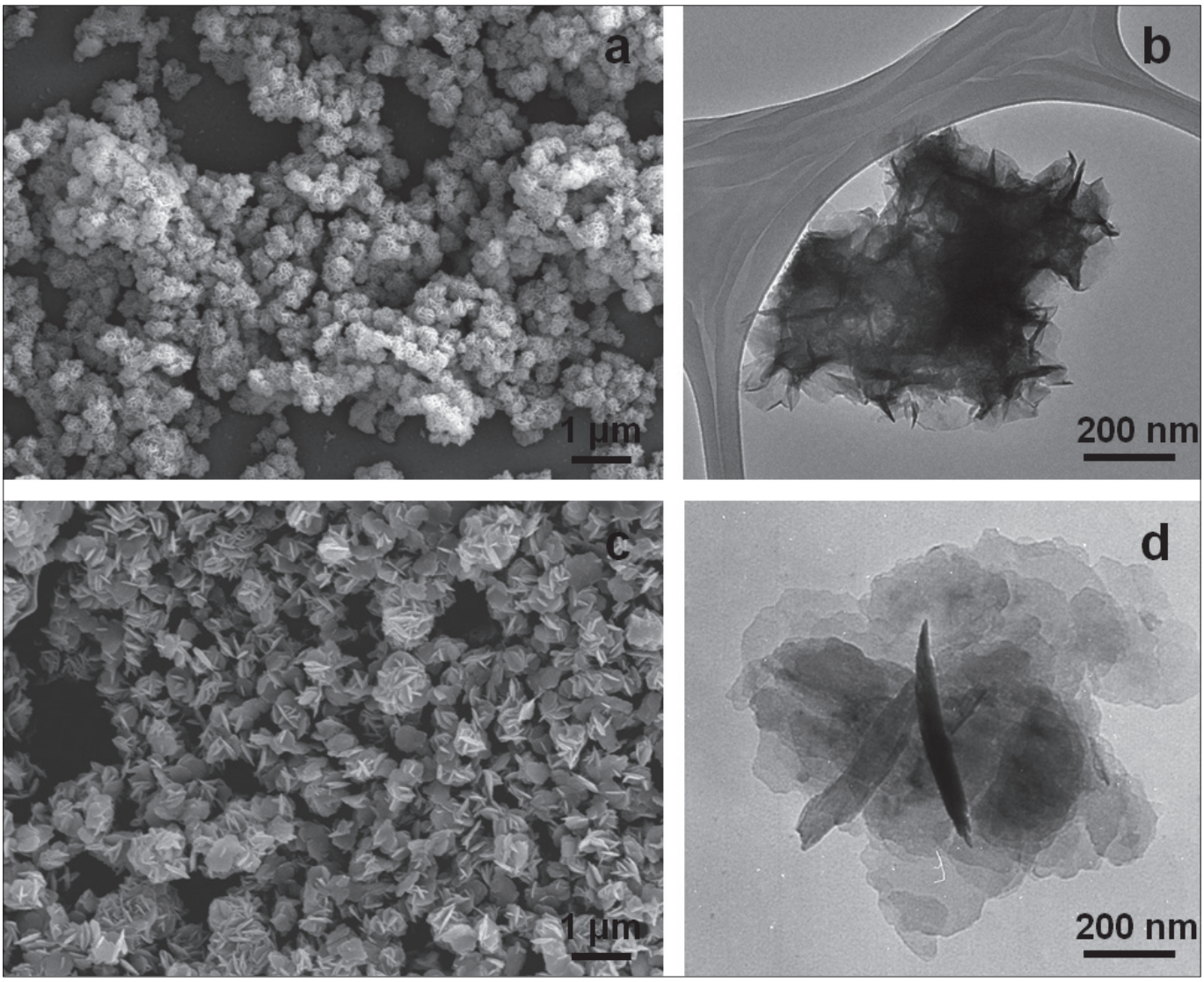

Figure 2. FESEM and TEM micrographs of samples ANH (a y b) and BNH (c y d).

previously calculated (being around 30 nm for sample ANH and 50 nm for sample BNH), as it can be also observed in the TEM images of figure 2 (figs. 2b and 2d)

The normalized FTIR spectra of both powders are shown in figure 3, where three significant differences can be observed. On the one hand, sample ANH present a wide band centered at 3450 cm^{-1}, while for sample BNH, this band appears as a well-defined peak centered at 3639 cm^{-1}, followed by a low intensity shoulder. Bands that appear in this area of the spectrum are assigned to stretching vibrations of the O-H bond. In the case of sample BNH, the narrow band is due to the hydroxyl groups that are bonded to nickel atoms and are part of the $Ni(OH)_2$ structure, while in the adjacent shoulder is associated to adsorbed water in the powder surface. However, in the case of sample ANH, the widening of the band indicates the presence of free hydroxyl groups, i. e. not bonded to nickel. These free OH groups are a consequence of the structural disorder inherent of a turbostratic phase, whose basal planes are not perfectly align among them but deviated from one another. This disorder opens the possibility to contain foreign molecules or ions from the reaction media inside the alpha phase structure [19]. This way, the hydroxyl groups can remain in the outside of the basal planes and generate inter- and intramolecular hydrogen bonds. The second difference between the FTIR spectra is the wavenumber at which $\delta_{Ni\text{-}O\text{-}H}$ and $\nu_{Ni\text{-}O}$ bands appear (662 y 490 cm^{-1} for sample ANH and 547 and 468 cm^{-1} for sample BNH, respectively). In the case of the

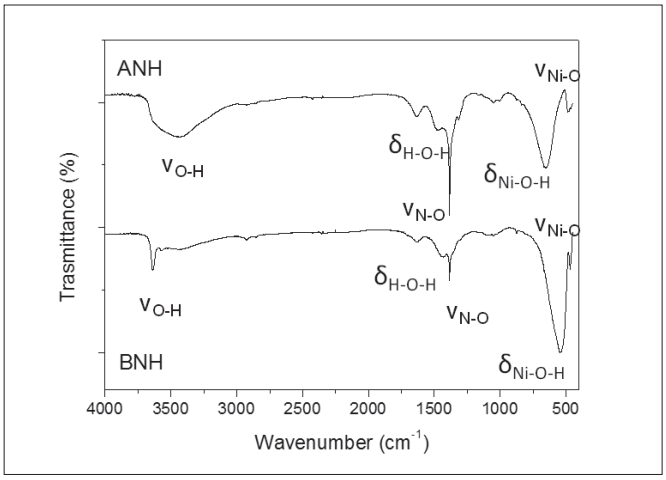

Figure 3. Normalized FTIR spectra of samples ANH and BNH.

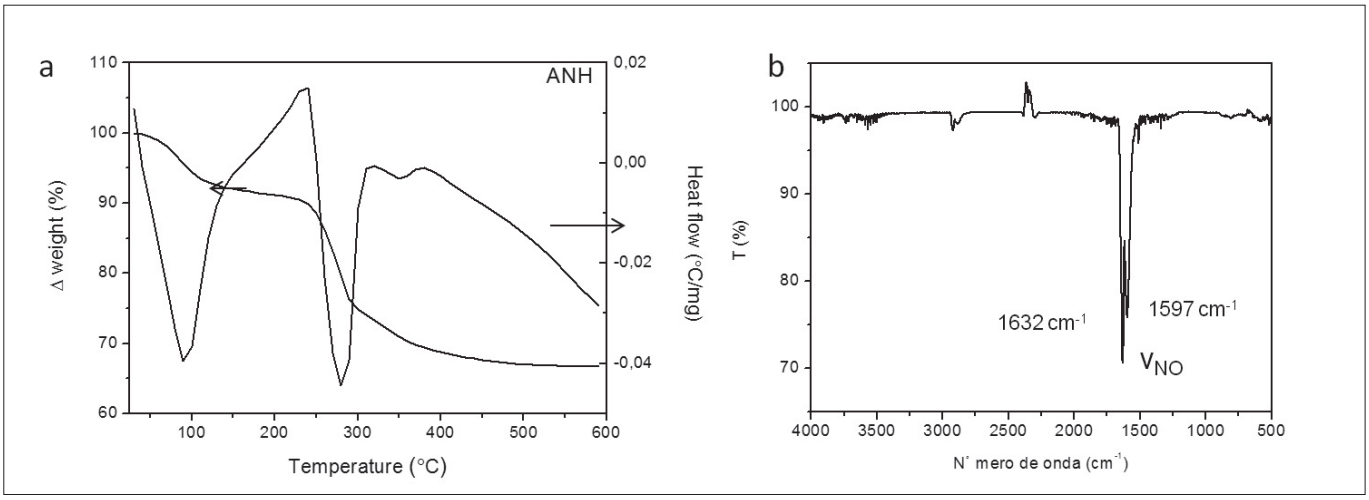

Figure 4. a) DSC-TGA curve and b) IR spectrum of the gases generated during the heat treatment of sample ANH that show the presence of nitrate ions trapped inside the alpha polymorph.

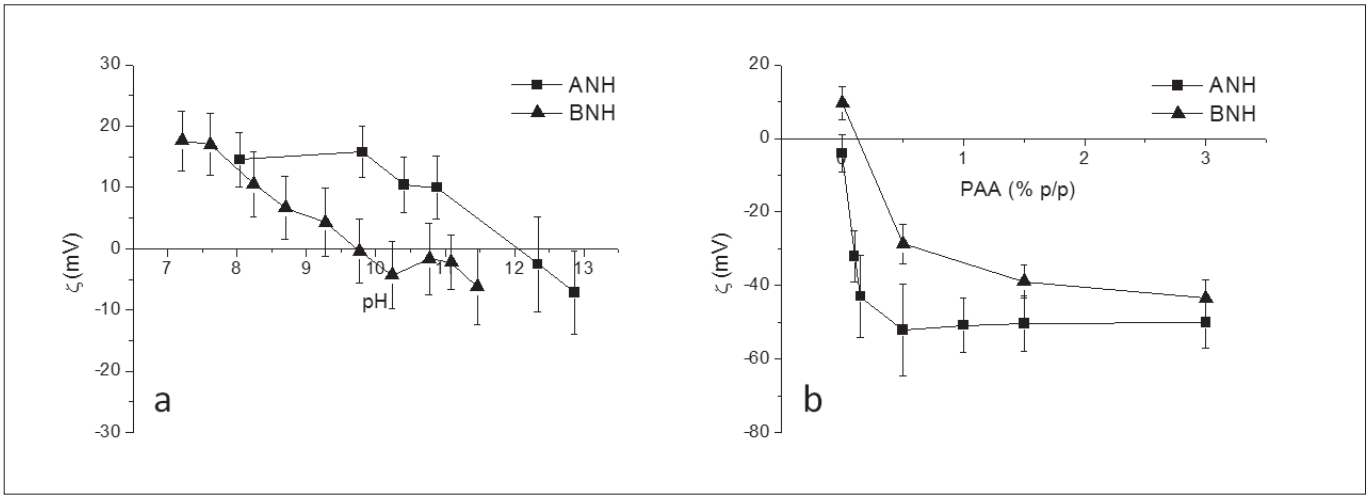

Figure 5. a) Zeta potential *vs*. pH curves of samples ANH and BNH where the IEP can be inferred, and b) saturation curves (zeta potential *vs*. PAA content) where the optimal PAA content is shown for both polymorphs.

beta phase, these wavenumbers agree with the ones reported in the literature [20]. However, the shift to higher values in the case of the alpha phase indicates a higher strength of the Ni-O bond due to a deficiency of hydroxyl groups in this polymorph that generates a higher positive charge density and, therefore, a stronger bond between the OH groups and the nickel cations. Finally, it can be observed that the intensity of the stretching band of the N-O band that appears at 1384 cm^{-1}, is different for the two samples. This band is a consequence of the nickel precursor used in the synthesis, i. e. $Ni(NO_3)_2{\cdot}6H_2O$, that can remain in small extent in the powder surface even after washing and drying. In the case of sample ANH, the higher intensity of the band is due to the nitrate ions (NO_3^-) that are trapped in the interplanar space of the alpha phase, as well as on its surface (as it happens for the beta polymorph), giving the alpha phase its turbostratic character. The presence of these anions can be corroborated by the presence of a small peak centered at 355 ºC in the DSC-TGA curve of sample ANH (fig. 4a), that corresponds to the decomposition of NO_3^- anions trapped in the alpha phase. The IR analysis of the gases generated during the heating process (fig. 4b) reveal the presence of nitrogen dioxide (NO_2) that comes from the decomposition of the NO_3^- anions.

3.2. Colloidal stability of $Ni(OH)_2$

Once the structure of the synthesized powders has been studied, and before their incorporation in the alumina matrix, their colloidal stability has been evaluated, and the influence of the morphological differences between both polymorphs in their colloidal stability has been discussed in detailed.

Figure 5a shows the isoelectric points (IEP, pH value at which the zeta potential becomes zero and so the suspension reaches its maximum instability) of samples ANH and BNH. In the case of sample BNH, the IEP was found to be 9.7, what is in good agreement with the values previously reported by Meyer *et al.* [16] and Durand-Keklikian *et al.* [15], while in the case of simple ANH, the IEP was established around 12. Due to the low chemical stability of the alpha phase, there are not previous values of its IEP in the literature. However, a series of IEP data published by Parks in 1965 points out that the IEP point of nickel hydroxide obtained by direct precipitation of a Ni^{2+} salt with NaOH is approximately 12, although the nickel hydroxide phase is not specified [21]. The difference in more than two units between the IEP of both polymorphs relies in the OH^- deficiency of the alpha phase. Despite the presence of NO_3^- that help keeping the electroneutrality of the compound,

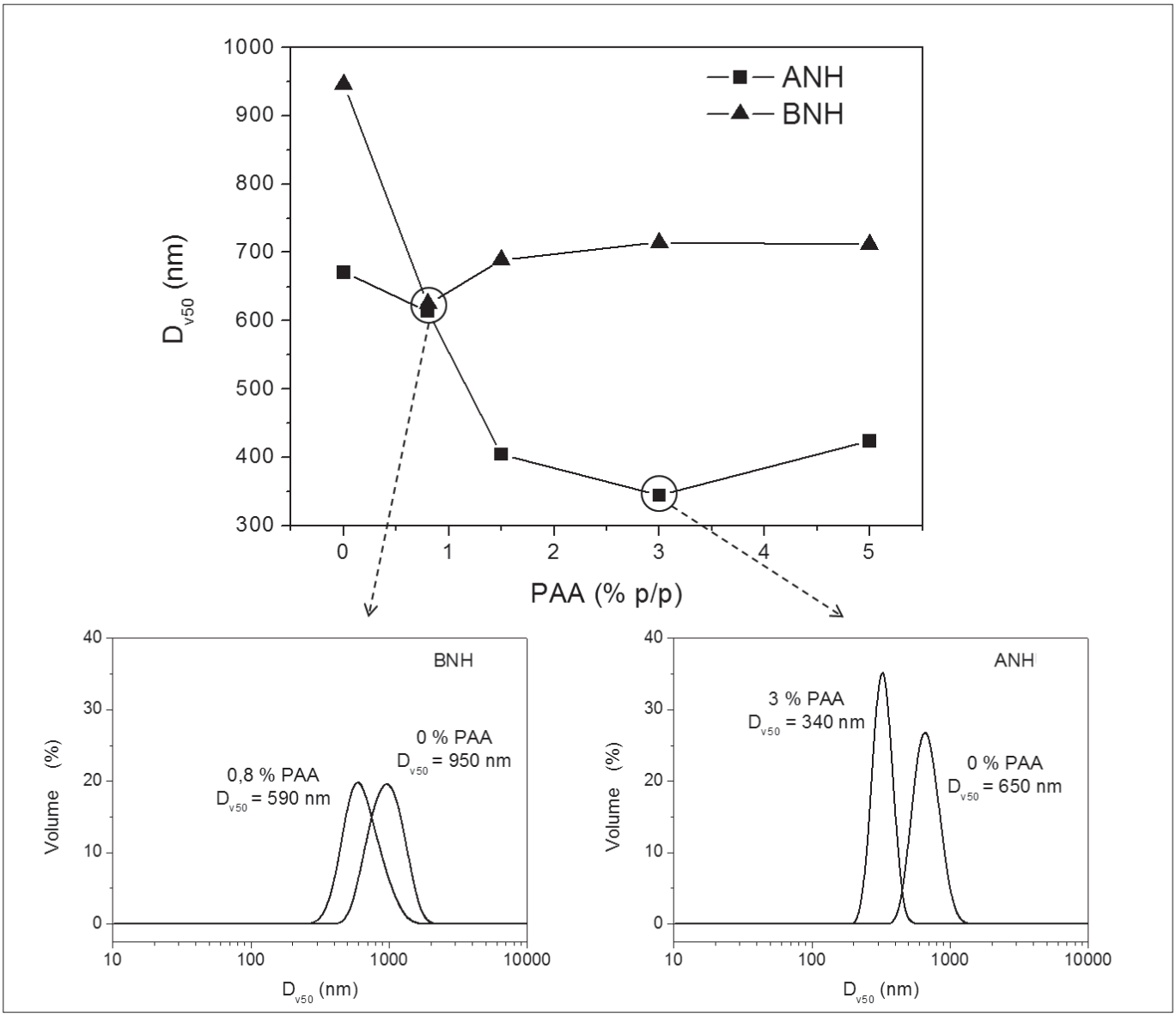

Figure 6. Particle size of sample ANH and BNH as a function of PAA content (up), and particles size distribution in volume in absence and with the optimal PAA content (down).

these anions are not integrated within the crystalline net but trapped between the different $Ni(OH)_2$ layers. This way, the surface of this powder (sample ANH) presents a higher density of positive points in its surface (due to the previously mentioned lack of OH^- groups) which makes it necessary to reach higher pH values to neutralize the surface charge.

Based on the equilibrium diagram of Ni^{2+} in water, that predicts the nickel hydroxide dissolution at pH ≤ 7.6 for a [Ni^{2+}] = 0.1 /L [22], and on the IEP of figure 5a, the working pH was established at around 9.5 to evaluate the dispersion capacity of PAA. At this pH value, both powders present a positive zeta potential, being the one of sample ANH much higher than the one for sample BNH due to the higher positive points on the surface of the alpha polymorph. The zeta potential *vs*. PAA (wt. %) measurements for both powders are shown in fig. 5b. As it can be seen, the optimal amount of PAA to disperse the powder suspension is different depending on the polymorph. While in the case of sample BNH a PAA content of 0.8 wt % is necessary to stabilize its zeta potential, sample ANH requires 3.0 wt. % of PAA. Moreover, the absolute zeta potential value for the beta phase is higher than that of the alpha phase, as it would be expected considering the low chemical stability of the alpha polymorph. The difference between the PAA quantities necessary to reach the optimal dispersion for both powders is mainly due to the difference in the specific surface area values (table 1), as well as to the higher positive points on the surface of sample ANH. The influence of these parameters can be explained if one considers that the stabilization mechanism when using polyelectrolytes such as PAA, passes through the electrostatic interaction of the charged polymer chains and the colloid, which implies that the higher the coordination points (which grows with the specific surface are), the higher the dispersant molecules that can be adsorbed on the surface of the particles.

The surface behavior of the powders is also revealed in the particles size obtained for each one using different PAA contents (fig. 6). The first thing that can be observed in figure 6 is that the smaller particles size for both ANH and

Bol. Soc. Esp. Ceram. Vidr. Vol 53. 6, 265-274, Noviembre-Diciembre 2014. ISSN 0366-3175. eISSN 2173-0431. http://dx.doi.org/10.3989/cyv.322014

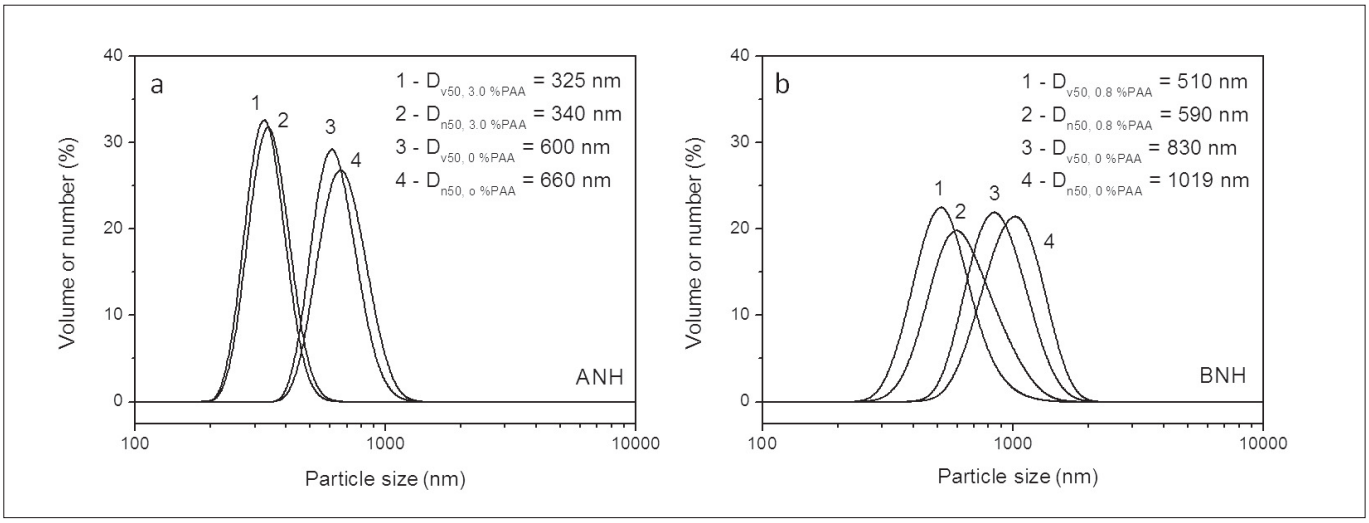

Figure 7. Particle size distribution in number and volumen of samples ANH (a) and BNH (b).

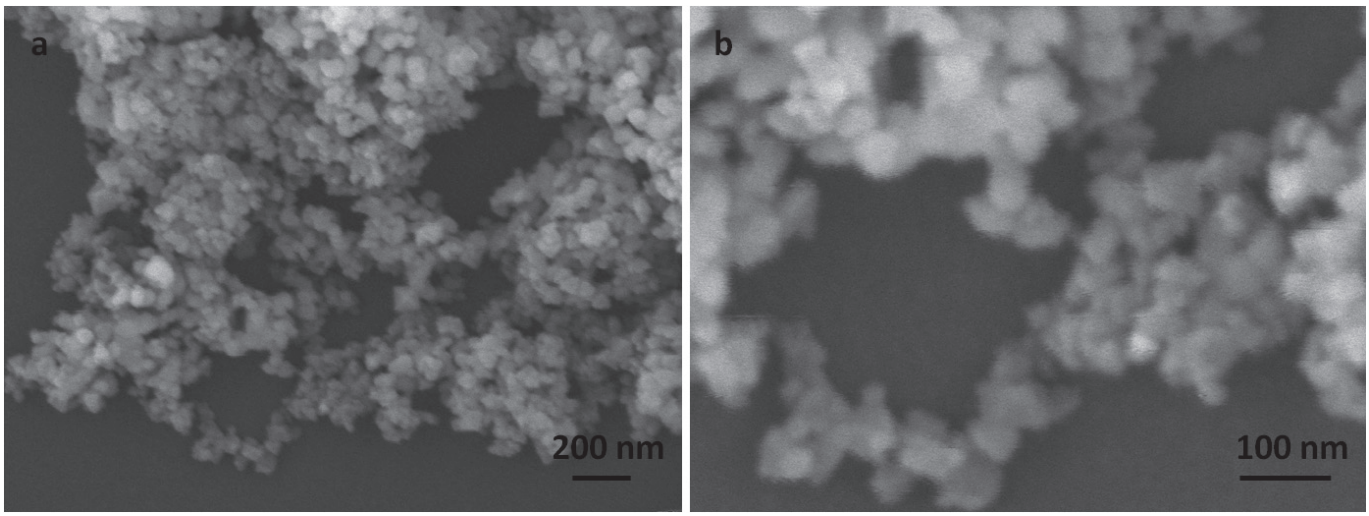

Figure 8. FESEM micrographs of metallic nickel particles obtained after the calcination process of simple ANH at 450 ºC using a reducing atmosphere (N_2/H_2 with 2 vol. % of H_2).

BNH samples us achieved when the optimal PAA content to stabilize the suspensions (previously calculated) is employed. This means 0.8 wt. % of PAA for sample BNH and 3.0 wt. % of PAA for sample ANH. The particle size distribution (in volume) in the absence and with the optimal PAA content is also shown in figure 6. From these graphs the decrease on the particles size when adding the optimal PAA content is observed. For sample BNH, the addition of 0.8 wt. % of PAA helps reducing the particle size from around 1 μm to approximately 590 nm, while in the case of sample ANH, the particle size can be decreased from 660 nm to 340 nm when 3.0 wt. % is added to the suspension. The second relevant fact that can be taken from figure 6 is the difference in the particle size distribution width of sample ANH and BNH. As it is observed, sample ANH presents a narrower distribution than sample BNH, which is related to the synthesis method employed in each case. On the hand, sample ANH was instantly synthesized by saturation of an ammonia solution using nickel. This rapid saturation leads to a high nucleation rate and to a short crystal growth, what results in homogeneous particles and, therefore, in a narrow size distribution. On the hand, the synthesis of sample BNH is carried out for longer times what makes the nucleation and crystal growth processes overlap in time leading to heterogeneous particles with a broad size distribution.

The size distribution functions in both number and volume are shown in figure 7. As it is observed, in the case of sample ANH, when using 3.0 wt. % of PAA both curves are practically coincident implying that a maximum dispersion has been reached and so that the aggregates in sample ANH cannot further divided into smaller fractions in this conditions. However, for sample BNH the size distribution I number and volume do not match when using 0.8 wt. % of PAA. This means that the maximum dispersion conditions are not reached probably due to the formation of strong aggregates during the synthesis with ultrasound, which cannot be divided into smaller ones.

3.3. Shaping and sintering of Ni/Al_2O_3 composites

After the evaluation of the colloidal stability of the powders it was established that the alpha phase presents smaller particle size and a better dispersion in aqueous media, therefore, the alpha phase was selected to be incorporated to the alumina

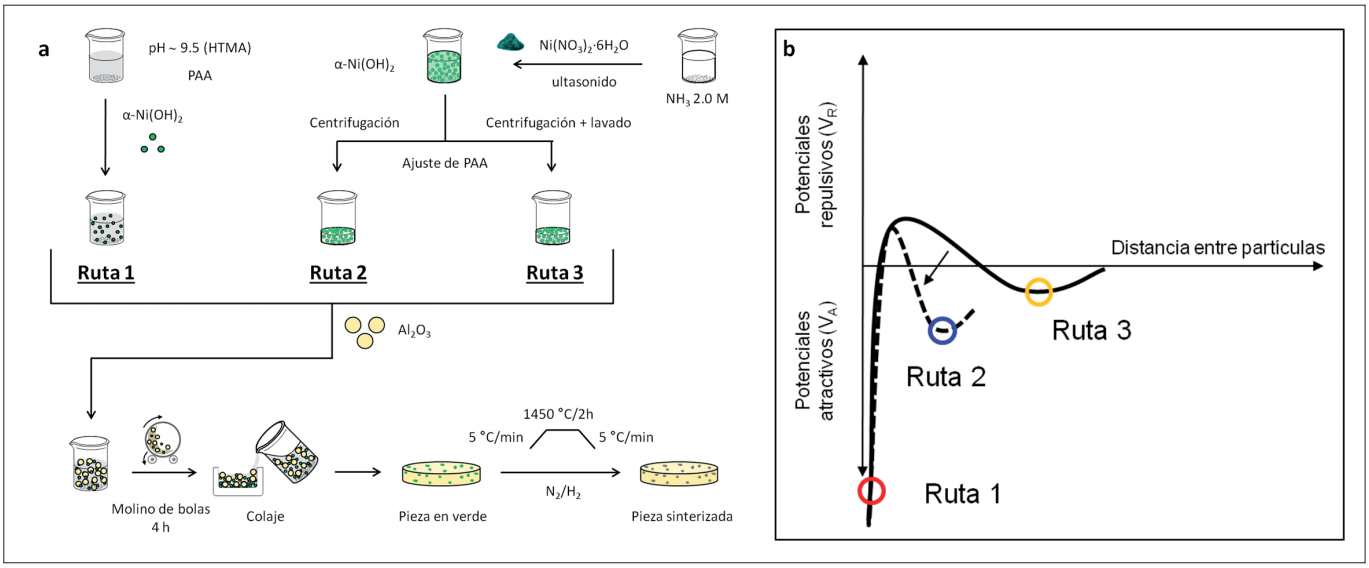

Figure 9. a) Processing scheme for the different colloidal routes and b) particle distance *vs*. potential diagram where the three different routes have been highlighted.

TABLE 2. DENSITY VALUES OF SAMPLES OBTAINED BY SLIP CASTING BEFORE AND AFTER SINTERING. THE THEORETICAL VALUE OF THE FINAL COMPOSITE WAS CONSIDERED 3.8 G/CM³.

Sample	Green samples		Sintered samples			
	$\rho_{(mercury)}$		$\rho_{(water)}$		$\rho_{(mercury)}$	
	g/cm³	% ρ_{th}	g/cm³	% ρ_{th}	g/cm³	% ρ_{th}
Ni/Al_2O_3-1	2.3	60	3.6	95	3.6	95
Ni/Al_2O_3-2	1.8	47	3.3	87	3.2	84
Ni/Al_2O_3-3	1.7	45	3.2	84	3.0	79

matrix. Taking into account that the sintering process to obtain Ni/Al_2O_3 composites is then carried out under reducing atmosphere, the morphology of the calcination products of the α-Ni(OH)$_2$ in such atmosphere (N_2/H_2 with 2 vol. % of H_2) at 450 ºC were studied (fig. 8). As it is observed (fig. 8a), the calcination process does not keep the sponge-like morphology of the alpha phase but results in the fragmentation of such structures. This way, and according to fig. 8b, discrete nickel particles with particles sizes around 50 nm are obtained.

Ni(OH)$_2$/Al_2O_3 suspension were prepared following three different processing routes, as shown in figure 9a, each one starting with the α-Ni(OH)$_2$ in a different part of the particles distance *vs*. potential curve of fig 9b.

For route 1, dry α-Ni(OH)$_2$ powder, which is considered to be highly agglomerated and therefore on the primary minimum of the curve, was employed. In the case of route 2, after the synthesis of the powder it was centrifuged (to eliminate the remains of the liquid) and used directly to fabricate the Ni(OH)$_2$/Al_2O_3 composites. This way, the ionic concentration of the media is high and so the powder is on the displaced secondary minimum where the distance between particles is smaller than for the original secondary minimum and the suspension is considered flocculated. Finally, in route 3 the powder was also used after the synthesis but in this case it was centrifuged and washed several times to decrease the ionic strength of the media. This way, it was considered to be in the original secondary minimum placed at longer distances between particles where the strength of the aggregates is relatively weak. Samples obtained through routes 1, 2 and 3 have been labeled Ni/Al_2O_3-1, Ni/Al_2O_3-2 and Ni/Al_2O_3-3, respectively.

The density of the green samples measured by the Archimedes method in mercury is shown in table 2. The smaller green density of samples Ni/Al_2O_3-2 and Ni/Al_2O_3-3, in comparison to simple Ni/Al_2O_3-1, can be explained considering that in routes 2 and 3 the nickel hydroxide particles were not dried and therefore they still keel their open morphology (sponge-like morphology). This open morphology avoids the free movement of the alumina particles within the suspension. On the contrary, in route 1 where the powder was previously dried, the nickel hydroxide is presented in a more compacted form that allows higher mobility for the alumina powder and therefore a better packing. This hypothesis needs to be corroborated by rheological studies that may shed light on the flow behavior at both low and high shear rate.

The density values of the sintered samples are also shown in table 2. As it is observed, the density value for sample Ni/Al_2O_3-1, where the starting nickel hydroxide was dry, reaches 95 % of the theoretical density, while for samples processes directly from the post-reaction media, the density does not reach 90 %. This smaller density of the sintered samples is in agreement with the smaller values observed for the green density. Values obtained in mercury and water barely differ from one another in the case of samples Ni/Al_2O_3-1 and Ni/Al_2O_3-2, which would indicate the existence of a close porosity. However, for sample Ni/Al_2O_3-3 the density measure in mercury is smaller than the one measured in water, indicating

Bol. Soc. Esp. Ceram. Vidr. Vol 53. 6, 265-274, Noviembre-Diciembre 2014. ISSN 0366-3175. eISSN 2173-0431. http://dx.doi.org/10.3989/cyv.322014

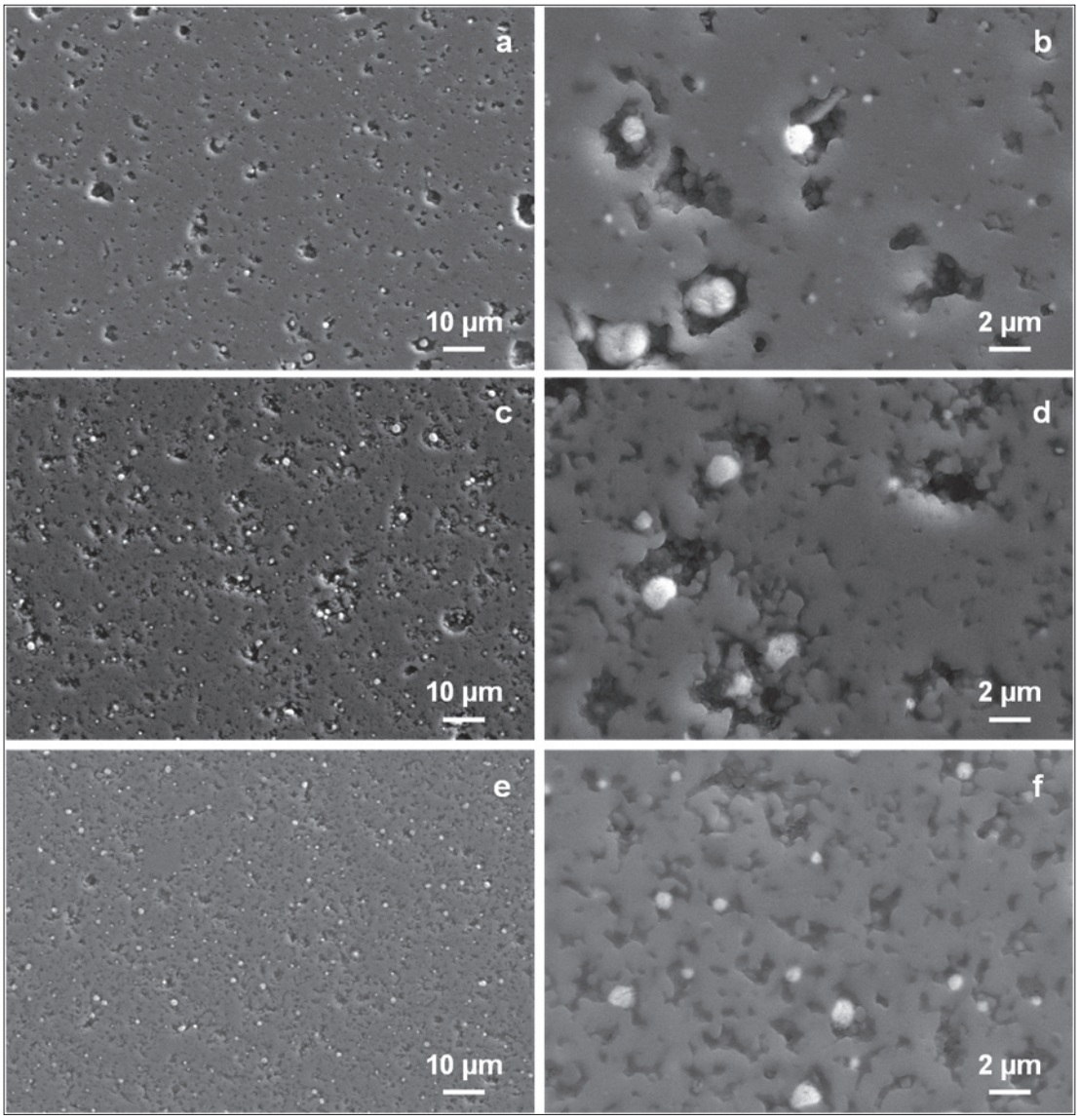

Figure 10. FESEM images of sintered samples Ni/Al_2O_3-1 (a, b) Ni/Al_2O_3-2 (c, d) and Ni/Al_2O_3-3 (e-f) corresponding to routes 1, 2 and 3, respectively.

that apart from the close porosity, there is also a small portion of open porosity in these samples.

The polished surface of the sintered samples observed by FESEM corroborates the higher porosity of samples Ni/Al_2O_3-2 and Ni/Al_2O_3-3 (fig. 10 c-f) compared to sample Ni/Al_2O_3-3 (fig. 10 a and b). In these images it is also shown how the pores and nickel particles distribution is different depending on the processing route. This way, in sample obtained by route 1 (Ni/Al_2O_3-1) close pores ranging from 2 to 10 μm are observed. In the inside of the biggest pores nickel particles with sizes larger than 2 μm are located. The space between the nickel and the alumina matrix indicates that the shrinkage of nickel agglomerates during sintering is higher than the one suffered by the matrix. This higher shrinkage is due to the spongy-like structure of the nickel hydroxide used in these conditions. The reducing effect created by hydrogen and the temperature of the sintering process make the discrete nickel particles join together by a coalescence mechanism that is also promoted by the diffusion ability of nickel at high temperatures. Besides, in the case of sample Ni/Al_2O_3-1 (fig. 10 b), a series of nickel particles with sizes between 100-200 nm embedded within the denser part of the alumina matrix is also observed, which probably resulted from the drying and milling processes. On the other hand, samples prepared by route 2 (Ni/Al_2O_3-2) present a higher porosity (fig. 10 c and d), even though the pore size is smaller than for samples prepare by route 1. Similarly to sample Ni/Al_2O_3-1, nickel particles are located in the inside of the largest pores. However, in sample Ni/Al_2O_3-2, nickel particle size is below 2 μm and a good distribution along the alumina matrix is observed. Nevertheless, in the dense areas of the alumina matrix no nickel particles with sizes between 100-200 nm are observed, as there were in sample Ni/Al_2O_3-1. Finally, the microstructure of sample processed through route 3 (Ni/Al_2O_3-3, fig. 10 e and f) presents nickel particles ranging from 0.5 to 1 μm homogeneously distributed in an alumina matrix with high degree of small porosity. As it happened with sample Ni/Al_2O_3-2, no discrete nickel particles of 100-200 nm are observed.

According to the final microstructure of the samples it should be highlighted that the three colloidal routes followed in this work led to homogeneous dispersions of nickel particles within an alumina matrix, which indicates the viability of these methods in the incorporation of metal precursors in ceramic

matrices. When drying the initial metal precursor (route 1), two apparently opposite phenomena are observed. On the one hand, nickel agglomerates are larger leading to final nickel particles bigger than 2 μm, while on the other side much smaller particles (100-200 nm) are observed in the composites, probably due to the brittleness acquired by the nickel hydroxide agglomerates during the drying process. When the drying process is avoided (routes 2 and 3), particles below 2 μm are obtained although no small discrete particles (100-200 nm) are observed. This is probably due to the fact that the synthesis media confers sufficient internal cohesion to the $Ni(OH)_2$ particles to maintain partial agglomeration of nanoparticles that cannot be broken in the experimental conditions covered in this work. In order to optimize the validated method presented here, it is necessary to go dipper in the optimization of the milling process, as well as to study the reology of the suspensions. Nevertheless, it could be concluded that avoiding the drying process, the agglomeration of the particles is also avoided and, therefore, the particle size of the metallic phase dispersed within the ceramic matrix decreases and becomes closer to the initial particle size of the synthesized powders.

4. CONCLUSIONS

Colloidal stability of α- and β-$Ni(OH)_2$ polymorphs, synthesized with the aid of ultrasound from an aqueous media, has been studied in detailed considering the cristalographic and morphological differences between the two phases. Taking into account the chemical stability of the nickel hydroxide in water, the optimal dispersion conditions of the powders have been established through zeta potential measurements using and anionic dispersant (PAA). This way, the IEP of the α-$Ni(OH)_2$ was established at around 10 while the optimal PAA content to stabilize the powder was found to be 3.0 wt. %. In the case of β-$Ni(OH)_2$ the IEP was found to be 9.7 and the optimal PAA content 0.8 wt. %. The different colloidal behaviors of the two polymorphs have been explained considering their crystallinity, specific surface area and the turbostratic character of the alpha phase, by means of FTIR and DTA-TG measurements.

Based on particle size measurements, it has been demonstrated that it is possible to achieve a maximum dispersion for the α-$Ni(OH)_2$, therefore this powder was chosen to be integrated into an alumina matrix by slip casting of concentrated suspensions. For that, three different processing routes have been studied depending on the strength and the agglomeration/aggregation degree of the $Ni(OH)_2$ particles, and three different Ni/Al_2O_3 composites have been obtained. In all cases, the metallic phase was highly dispersed in the ceramic matrix, being the size of the nickel particles smaller when the drying process is avoided and the powder is washed before mixing with alumina (route 3). The density of the sintered materials and the analysis of their microstructure allows to evaluate the influence of the strength of agglomerates and aggregates on the quality of the final composite materials.

AKNOWLEDGEMENTS

The authors would like to acknowledge the Spanish Government support under projects MAT2012-38650-C02-02.

BIBLIOGRAPHY

1. Low, I. M. (2006): Ceramic matrix composites. Microstructure, properties and applications. Woodhead Publishing Limited, Cambridge, UK.
2. Wang, Y; Peng, J; Zhou, C; Lim, Z-Y; Wu, C; Ye, S; (2014): Effect of Pr addition on the properties of Ni/Al2O3 catalysts with an application in the autothermal reforming of methane, *Int. J. Hydrogen Energy* 39 (2): 778–787. http://dx.doi.org/10.1016/j.ijhydene.2013.10.071
3. Gonzalo-Juan, I; Ferrari, B; Colomer, M.T and Sanchez-Herencia, A. J; (2010): Colloidal processing and sintering of porous percolative Ni-YSZ layers, *J. Memb. Sci.*352 (1-2): 55–62. http://dx.doi.org/10.1016/j.memsci.2010.01.060.
4. Zhu, W. Z; Deevi, S. C; (2003): A review on the status of anode materials for solid oxide fuel cells, *Mater. Sci. Eng. A* 362 (1-2): 228–239. http://dx.doi.org/10.1016/S0921-5093(03)00620-8
5. Moya, J.S; Lopez-Esteban, S; and Pecharroman, C; (2007): The challenge of ceramic/metal microcomposites and nanocomposites, *Prog. Mater. Sci.* 52 (7): 1017–1090. http://dx.doi.org/10.1016/j.pmatsci.2006.09.003
6. Ferrari, B; Sanchez-Herencia, A. J; Moreno, R; (2006): Nickel-alumina graded coatings obtained by dipping and EPD on nickel substrates, *J. Eur. Ceram. Soc.* 26 (12): 2205–2212. http://dx.doi.org/10.1016/j.jeurceramsoc.2005.04.009
7. Sanchez-Herencia, A.J; (2007): Water based colloidal processing of ceraic laminates, *Key Eng. Mater.* laminates, 333: 39–48. http://dx.doi.org/10.4028/www.scientific.net/KEM.333.39.
8. Gonzalo-Juan, I; Escribano, J. A; Castro, Y; Sanchez-Herencia, A.J; Fierro, J. L. G; Ferrari, B; (2014): One-pot manufacture of nanoparticle-based films in aqueous media via an electric field-driven assembly process, *Green Chem.*16 (6): 3286–3296. http://dx.doi.org/10.1039/C3GC42539hH.
9. Jeevanandam, P; Koltypin, Y; Gedanken, A; (2001): Synthesis of nanosized alpha-nickel hydroxide by a sonochemical method, *Nano Lett.* 1 (5): 263–266. http://dx.doi.org/10.1021/nl010003p.
10. Soler-illia, G. J. D. A. A; Regazzoni, A.E; Blesa, M.A; (1999): Synthesis of Nickel Hydroxide by Homogeneous Alkalinization . Precipitation Mechanism, *Chem. Mater.* 11 (11): 3140–3146. http://dx.doi.org/10.1021/cm9902220.
11. Xu, L; Ding, Y; Chen, C; Zhao, L; Rimkus, C; Joesten, R; (2008): 3D Flowerlike α -Nickel Hydroxide with Enhanced Electrochemical Activity Synthesized by Microwave-Assisted Hydrothermal Method, *Chem. Mater.* 20 (1): 308–316. http://dx.doi.org/10.1021/cm702207w.
12. Cabanas-Polo, S; Suslick, K. S; Sanchez-Herencia A. J; (2011): Effect of reaction conditions on size and morphology of ultrasonically prepared Ni(OH)(2) powders, *Ultrason. Sonochem.*18 (4): 901–906. http://dx.doi.org/10.1016/j.ultsonch.2010.11.017.
13. Kiani, M. A; Mousavi, M. F; Ghasemi, S; (2010): Size effect investigation on battery performance: Comparison between micro- and nano-particles of β-Ni(OH)2 as nickel battery cathode material, *J. Power Sources*, 195 (17): 5794–5800. http://dx.doi.org/10.1016/j.jpowsour.2010.03.080.
14. Palacín, M.R; (2009): Recent advances in rechargeable battery materials: a chemist's perspective, *Chem. Soc. Rev.*38 (9): 2565–2575. http://dx.doi.org/10.1039/b820555h.
15. Durand-Keklikian, L; Haq, I; Matijevic, E; (1994): Preparation and characterization of well-defined colloidal nickel compounds, *Colloids Surf., A*, 92: 267–275. http://dx.doi.org/10.1016/0927-7757(94)02952-0.
16. Meyer, M; Bée, A; Talbot, D; Cabuil, V; Boyer, J. M; Répetti, B; (2004): Synthesis and dispersion of Ni(OH)2 platelet-like nanoparticles in water, *J. Colloid. Interface Sci.* 277 (2): 309–415. http://dx.doi.org/10.1016/j.jcis.2004.04.034.
17. Bowen, P; Carry, C; Luxembourg, D; Hoffmann, H; (2005): Colloidal processing and sintering of nanosized transition aluminas, *Powder Technol.*157 (1-3): 100–107. http://dx.doi.org/10.1016/j.powtec.2005.05.015.
18. Sanchez-Herencia, A. J; Hernandez, N; Moreno, R; (2006): Rheological Behavior and Slip Casting of Al2O3-Ni Aqueous Suspensions, *J. Am. Ceram. Soc.*89 (6): 1890–1896. http://dx.doi.org/10.1111/j.1551-2916.2006.01045.x.
19. Delahaye-Vidal, A; Fligarz, M; (1987): Textural and structural studies on nickel hydroxide electrodes . II . Turbostratic nickel (II) hydroxide submitted to electrochemical redox cycling, *J. Appl. Electrochem.*17: 589–599. http://dx.doi.org/10.1007/BF01084134.
20. Xu, P; Han, H. J; Zhang, B; Lv, Z. S; Liu, X. R; (2007): Caracterization of ultrafine nickel hydroxide from supersonic co-precipitation method, *J. Alloys Compd.* 436 (1-2): 369–374. http://dx.doi.org/10.1016/j.jallcom.2006.07.055.
21. Parks, G. A; (1965): The isoelectric points of solid oxides, solid hydroxides and aqueous hydroxo complex systems, *Chem. Rev.*65 (2): 177–198. http://dx.doi.org/10.1021/cr60234a002.
22. Burriel Marti, F; Lucena Conde, F; Arribas Jimeno, S; Hernandez Mendez, J. (1983): Química analítica cualitativa. Paraninfo, Madrid, España.

Recibido: 26/11/2014
Recibida versión corregida: 11/12/2014
Aceptado: 11/12/2014